Journal of Catalysis 325 (2015) 111–117

Contents lists available at ScienceDirect

Journal of Catalysis

journal homepage: www.elsevier.com/locate/jcat

Platinum on carbonaceous supports for glycerol hydrogenolysis: Support effect

Werner Oberhauser [a,*], Claudio Evangelisti [b,*], Ravindra P. Jumde [b], Rinaldo Psaro [b], Francesco Vizza [a], Manuela Bevilacqua [a], Jonathan Filippi [a], Bruno F. Machado [c], Philippe Serp [c]

[a] Istituto di Chimica dei Composti Organometallici (CNR-ICCOM), Sesto Fiorentino 50019, Italy
[b] Istituto di Scienze e Tecnologie Molecolari (CNR-ISTM), Milano 20138, Italy
[c] Laboratoire de Chimie de Coordination, UPR CNRS 8241, Composante ENSIACET, Universitè de Toulouse UPS-INP-LCC, 4 allée Emile Monso, BP 44362, 31030 Toulouse Cedex 4, France

ARTICLE INFO

Article history:
Received 24 November 2014
Revised 27 January 2015
Accepted 5 March 2015

Keywords:
Hydrogenolysis
Glycerol
Metal vapor synthesis
Platinum nanoparticles
Carbonaceous supports

ABSTRACT

Metal vapor synthesis (MVS) technique was applied to generate Pt-nanoparticles of different size (<1.3 nm and 2.5 nm) deposited onto carbonaceous supports, mainly characterized by a different surface area. The supported catalysts were employed in the glycerol hydrogenolysis reaction carried out under basic reaction conditions at 433 and 453 K to obtain 1,2-propanediol as the main liquid product. Comparison of the composition of the liquid- and gas-phase products obtained by the different catalysts showed a clear dependence of aqueous-phase reforming, water–gas shift reaction activity as well as 1,2-propanediol chemoselectivity on the degree of Pt-sintering occurring on different carbon supports. High-resolution transmission electron microscopic and X-ray powder diffraction studies carried out on as-synthesized and recovered heterogeneous catalysts provided clear evidences that a high surface area carbon support, such as Ketjen Black EC-600JD, notably retards nanoparticle aggregation.

1. Introduction

The hydrogenolysis (*i.e.*, dehydration and successive hydrogenation) of glycerol, which is the major by-product of biodiesel production, brings about the formation of the value-added diols 1,2-propanediol (1,2-PD) [1–7] and 1,3-propanediol (1,3-PD) [8,9], which are mainly applied in the synthesis of biodegradable polymers, functional fluids, foods, cosmetics, and fragrances [10]. Glycerol (GLY) hydrogenolysis generally needs harsh catalytic conditions (*i.e.*, 400–500 K, basic reaction conditions and a dihydrogen pressure of 210–4500 psi) to proceed [10,11]. The activity of metal supported catalysts for glycerol hydrogenolysis follows the order Ru ≈ Cu ≈ Ni > Pt > Pd [11]. The main issue of glycerol hydrogenolysis reactions is related to the selective breaking of C–C or C–O bonds of the triol. In this respect, Pt shows generally much lower C–C hydrogenolysis activity compared to Ru, being hence a suitable candidate for the base-mediated chemoselective hydrogenolysis of GLY to 1,2-PD and lactate [5–7]. Along with the hydrogenolysis activity, aqueous-phase reforming (APR) is also observed, which is a structure sensitive process (*i.e.*, selectivity depends on metal particle size) [12–17]. Tomishige discussed a related nanoparticle (NP) size-sensitivity for the Ru-/C-mediated GLY hydrogenolysis reaction to give 1,2-PD as main product (*i.e.*, smaller particles were less selective for the 1,2-PD production) [4]. Directly connected to the selectivity problem is the stabilization of Pt-NPs in the course of the catalytic hydrogenolysis reaction. In this respect, the application of bimetallic Pt-Ru-NPs [7] and particle modification by additional ligands [18] did not really improve the performance of Pt-based catalysts. On the other hand, the nature of the support used notably influences the NPs' growth, since it behaves as a macroligand which interacts with the NPs' surface by its functional groups. Herein, we systematically study the effect of the support surface area on the sintering of Pt-NPs during glycerol hydrogenolysis reaction. To this purpose, we chose three graphite-type carbon supports, which differ mainly in surface area and atomic oxygen content (*i.e.,* Ketjen Black EC-600JD (C^K) (1396 m^2/g, 6.2%) [19], Vulcan XC-72 (C^V) (254 m^2/g, 5.4%) [19], and few layer graphene (C^G) (55 m^2/g, 3.9%) [20]. Pt-NPs of controlled size (<1.3 nm and 2.5 nm, respectively) were deposited on the different carbon supports by means of metal vapor synthesis (MVS) technique [21].

2. Experimental

2.1. Materials

GLY and NaOH were purchased from Aldrich and used as received. Mesitylene and *n*-pentane were purified by conventional

* Corresponding authors.
E-mail addresses: werner.oberhauser@iccom.cnr.it (W. Oberhauser), claudio.evangelisti@istm.cnr.it (C. Evangelisti).

http://dx.doi.org/10.1016/j.jcat.2015.03.003
0021-9517/

methods, distilled, and stored under argon. C^K and C^V were purchased from Cabot Corp. USA, while C^G was prepared as reported in the literature [20]. Water was bidistilled.

2.2. Catalyst preparation

The Pt-NPs supported onto C^K, C^V, and C^G were synthesized by the MVS technique as follows: Platinum vapors generated at 1.45×10^{-6} psi by resistive heating of a tungsten wire surface coated with electrodeposited platinum (ca. 102.0 mg) were co-condensed with either mesitylene or *n*-pentane (60.0 mL) in a glass reactor at 77 K. The reactor chamber was heated to the melting point of the solid matrix, and the resulting brown solution (55.0 mL) was kept under argon atmosphere in a Schlenk tube at 195 K. The Pt-content of the obtained Pt-solvated metal atoms (SMAs) was determined by ICP-OES (1.4 mg/mL for Pt/mesitylene and 0.6 mg/mL for Pt/*n*-pentane). The SMAs (33.0 mg of Pt, 24.0 mL of Pt/mesitylene, or 55.0 mL of Pt/*n*-pentane) were added to a dispersion of the support (1.10 g) in either mesitylene or *n*-pentane (20.0 mL). The resulting suspension was warmed up to 298 K under stirring for 12 h. Afterward the solvent was removed by vacuum and the obtained solids $Pt@C^K/C^V/C^G$ were washed with *n*-pentane and dried under reduced pressure. All isolated samples contained 3.0 wt.% of Pt as determined by ICP-OES analysis.

2.3. Catalyst characterization

Transmission electron microscopy (TEM) analysis of the supported Pt-NPs was carried out with a ZEISS LIBRA 200FE High-resolution Transmission Electron Microscope (HRTEM), equipped with a FEG source operating at 200 kV, in column second-generation omega filter for energy selective spectroscopy (EELS) and imaging (ESI), HAADF-STEM facility, EDS probe for chemical analysis, integrated tomographic HW and SW. The samples of the supported catalysts were ultrasonically dispersed in isopropanol and a drop of the suspension was deposited on a holey-carbon film supported on a copper TEM grid of 300 mesh. Histograms of the particle size distribution were obtained by counting at least 500 particles. The mean particle diameter (d_m) was calculated using the formula $d_m = \sum d_i n_i / \sum n_i$, where n_i is the number of particles with diameter d_i. Powder X-ray diffraction (PXRD) spectra were acquired at room temperature with a PANalytical X'PERT PRO powder diffractometer, employing Cu Kα radiation (λ = 1.5418 Å), and a parabolic MPD-mirror. The spectra were acquired in the 2Θ range from 5.0° to 100.0°, applying a step size of 0.0263° and a counting time of 70.9 s.

ICP-OES analyses of the supported catalysts were carried out with an iCAP 6200 Duo upgrade, Thermofisher instrument. A sample (1.0 mL) of Pt-SMA solution was heated over a heating plate in a porcelain crucible in the presence of aqua regia (2.0 mL) for six times, dissolving the solid residue in 0.5 M aqueous HCl. The limit of detection calculated for platinum was 2 ppb.

The BET-specific surface area of selected Pt-containing samples was determined by nitrogen adsorption at 77 K using a Micromeritics ASAP 2020 analyzer.

The metal dispersion and particle size of $Pt_a@C^K$, $Pt_b@C^K$, $Pt_a@C^V$, and $Pt_b@C^V$ was determined with the latter apparatus by dihydrogen chemisorption at 308 K in the pressure range between 0.09 and 9.7 psi. The sample was pretreated by a H_2 flow for 1.5 h at T_{red} of 423 and 473 K, followed by evacuation at $T_{evacuation} = (T_{red} + 10\,K)$ for 10 h. After cooling the sample to 308 K, it was again evacuated for 2 h and then analyzed at 308 K. The metal surface area was determined from the total amount of adsorbed H_2 at 308 K and then extrapolated to zero pressure, assuming a Pt/H stoichiometry equal to unity. The amount of chemisorbed gas on the sample surface was determined after subtracting the physisorbed contribution.

2.4. Catalytic hydrogenolysis reaction

Supported Pt catalysts $Pt_a@C^{K/V/G}$ (100.0 mg, 0.01538 mmol of Pt, *a* corresponds to a 87% Pt dispersion; 0.01338 mmol $Pt_{surface}$) and $Pt_b@C^{K/V}$ (164.0 mg, 0.02522 mmol of Pt, *b* corresponds to a 53% Pt dispersion; 0.01338 mmol $Pt_{surface}$) were introduced into a stainless steel autoclave, which was then sealed and evacuated. Afterward a deaerated solution of GLY (17.046 mmol) (*i.e.*, GLY to $Pt_{(surface)}$ molar ratio of 1274) and NaOH (40.0 mmol) in water (50.0 mL) was introduced into the autoclave by suction at room temperature. The autoclave was then charged with dihydrogen (600 psi) at 303 K and heated to the desired reaction temperature under agitation (1000 rpm). After the desired reaction time, the autoclave was cooled to room temperature and the gaseous reaction products were analyzed with a QIC Series Mass Spectrometer (Hiden Analytical). The residual gas pressure was then released, the autoclave opened, and the liquid phase neutralized with sulfuric acid (0.1 M) and afterward analyzed by high pressure liquid chromatography (HPLC) (*i.e.*, Shimadzu-UFLC apparatus, equipped with a RID detector and a Alltech OA-1000 organic acid column of 300 mm (length) and a 6.5 mm (i.d.); 0.01 N H_2SO_4 was used as eluent combined with a eluent flow rate of 0.4 mL/min at 338 K.

Supported catalysts were recovered by filtration, washed with water (3 × 10.0 mL) and acetone (2 × 10.0 mL), and then dried at room temperature.

Recovered $Pt_a@C^K$ and $Pt_a@C^V$ was used for recycling experiments carried out at 433 K.

The GLY conversion (%), the amount of gas-phase products (%), the chemoselectivity of the liquid products (%), and TOF values were determined as follows:

$$\text{GLY conversion } (\%) = [\text{mol}(GLY_{initial}) - \text{mol}(GLY_{unreacted})]/\text{mol}(GLY_{initial}) \times 100.$$

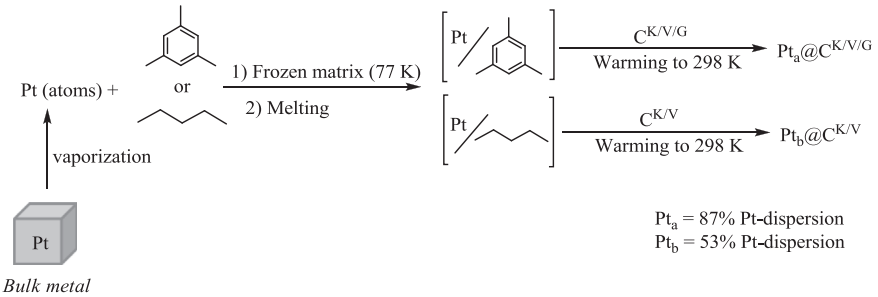

Scheme 1. Catalysts' synthesis by MVS technique.

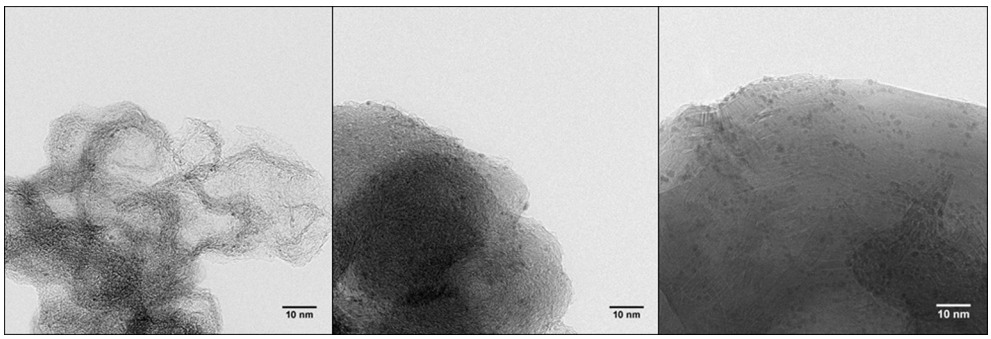

Fig. 1. HRTEM-micrographs of $Pt_a@C^K$ (left), $Pt_a@C^V$ (middle), and $Pt_a@C^G$ (right).

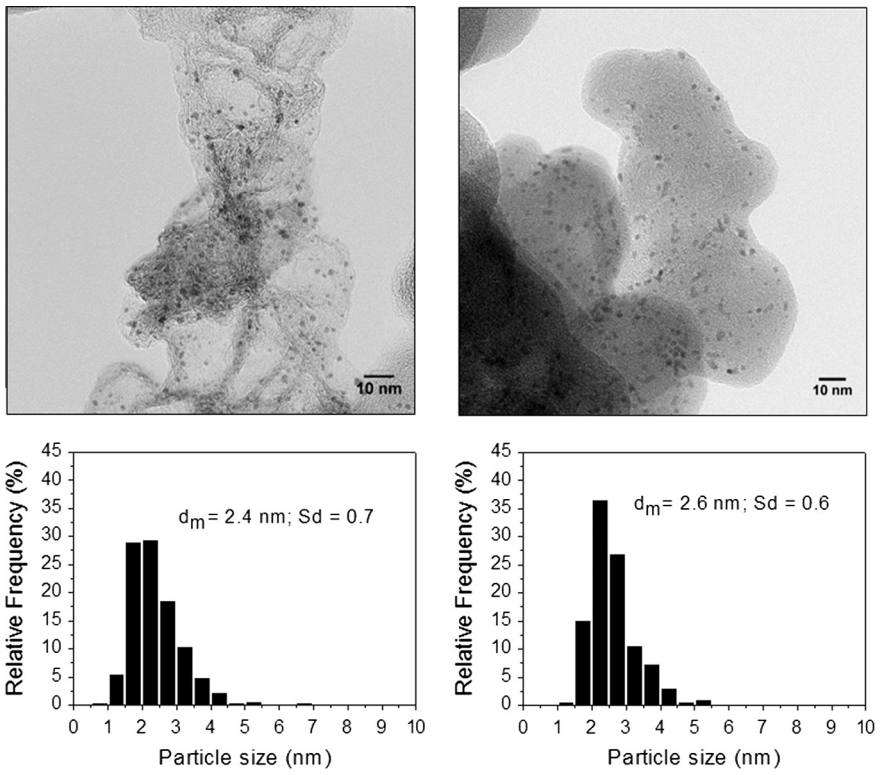

Fig. 2. HRTEM-micrographs and histograms of $Pt_b@C^K$ (left) and $Pt_b@C^V$ (right).

Amount of gas-phase products (%) = [mol($GLY_{initial}$) − mol($GLY_{unreacted}$) − Σmol(products)]/mol($GLY_{initial}$) × 100.
Chemoselectivity (%) = mol($_{product}$)/[mol($GLY_{initial}$) − mol($GLY_{unreacted}$)] × 100.
TOF = mol($GLY_{reacted}$)/[mol($Pt_{surface}$) × h] with a $Pt_{surface}$ amount of 13.37 × 10^{-3} mmol. TOF values are given after 4 and 8 h of reaction time.

3. Results and discussion

Pt-NPs were synthesized by MVS technique [21,22], as shown in Scheme 1. The MVS approach to obtain metal particles has generally the following advantages over traditional metal particle synthesis which foresees a reduction step of the oxidized metal precursor [23–25]: (*i*) The final Pt-content can be adjusted by the concentration of the solvated metal particles in solution; (*ii*) Pt-NPs of comparable size are accessible, regardless of the support employed; moreover, the size of the metal particles can be controlled upon the different metal clusters' growth in different

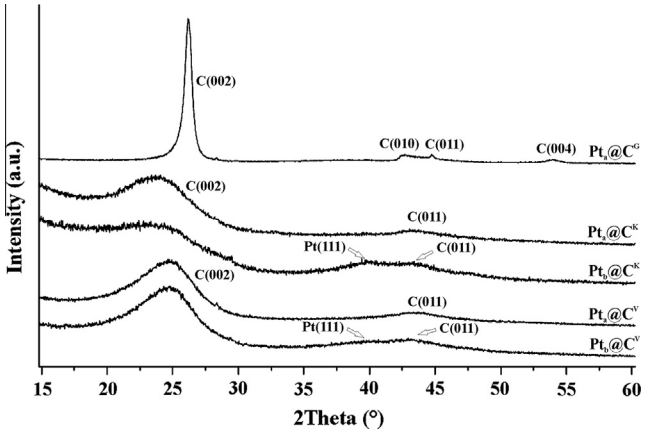

Fig. 3. PXRD diffractograms of the as-synthesized carbon-based Pt catalysts.

Table 1
N_2-physisorption measurements of $Pt_{a,b}@C^{K/V}$.

	Surface area (m^2/g)	Cumulative pore volume (cm^3/g)
C^K	1396.3	4.39
C^V	254.0	1.74
$Pt_a@C^K$	775.4	2.36
$Pt_a@C^K$[a]	743.1	2.36
$Pt_b@C^K$	984.0	3.20
$Pt_a@C^V$	147.1	0.62
$Pt_b@C^V$	191.0	0.74

[a] After catalysis 433 K, 4 h.

solvents; (*iii*) The supported NPs contain only metal in its reduced form. In order to obtain Pt-NPs of different size in solution, mesitylene and *n*-pentane were used as solvent. Indeed, it has been proved by NMR spectroscopy that mesitylene is capable of stabilizing very small Pt nanoclusters (<1.5 nm) in solution [26]. Unlike mesitylene, the non-coordinating property of *n*-pentane was exploited to prepare Pt-NPs of larger size. The simple addition of the desired support (*i.e.*, $C^{K/V/G}$) to the mesitylene or *n*-pentane-solvated Pt nanoclusters in solution gave the supported catalysts $Pt_a@C^{K/V/G}$ and $Pt_b@C^{K/V}$ as shown in Scheme 1.

Table 2
Catalytic hydrogenolysis of GLY with $Pt_a@C^{K/V/G}$ and $Pt_b@C^{K/V}$.

Entry[a]	Catalyst	Conv. (%)/TOF (h^{-1})	Gas-phase (%)	Liquid-phase chemoselectivity (%)			Gas-phase products distribution (%)		
				1,2-PD	EG	LA	CO	CO_2	CH_4
453 K									
1	$Pt_a@C^K$	82/261	27	60	4	1	89	11	Trace
2	$Pt_b@C^K$	30/96	4	69	–	–	91	8	1
3[b]	$Pt_b@C^K$	55/88	12	59	3	1	nd	nd	nd
4[c]	$Pt_a@C^V$	4/13	nd	nd	nd	nd	nd	nd	nd
5[d]	$Pt_a@C^V$	100/nd	54	–	–	47	nd	nd	nd
6[e]	$Pt_a@C^V$	17/54	13	–	–	23	nd	nd	nd
7	$Pt_a@C^V$	79/252	27	55	6	4	92	8	Trace
8	$Pt_b@C^V$	24/76	4	75	2	4	95	4	1
9[b]	$Pt_b@C^V$	40/64	12	55	1	1	97	2	1
10	$Pt_a@C^G$	49/156	33	21	<1	12	99	1	Trace
433 K									
11	$Pt_a@C^K$	57/181	14	73	7	–	85	14	1
12[f]	$Pt_a@C^K$	54/171	15	70	6	–	86	13	1
13[g]	$Pt_a@C^K$	52/165	17	68	6	–	88	10	2
14[b]	$Pt_a@C^K$	80/127	16	70	5	–	nd	nd	nd
15	$Pt_b@C^K$	15/48	6	60	–	–	93	6	1
16	$Pt_a@C^V$	53/169	22	53	2	4	84	15	1
17[f]	$Pt_a@C^V$	44/140	24	48	2	5	88	11	1
18[g]	$Pt_a@C^V$	39/124	23	40	1	4	nd	nd	nd
19[b]	$Pt_a@C^V$	57/90	27	43	3	5	nd	nd	nd
20	$Pt_b@C^V$	12/38	9	40	–	–	92	7	1

[a] Catalytic conditions: mmol GLY/mmol $Pt_{(surface)}$ = 1274, H_2O (50.0 mL), GLY (17.046 mmol), NaOH (40.0 mmol), p(H_2) (600 psi at 303 K), *t* (4 h).
[b] 8 h.
[c] In the absence of NaOH.
[d] In the absence of H_2.
[e] 1,2-PD instead of GLY.
[f] 1st recycle.
[g] 2nd recycle.

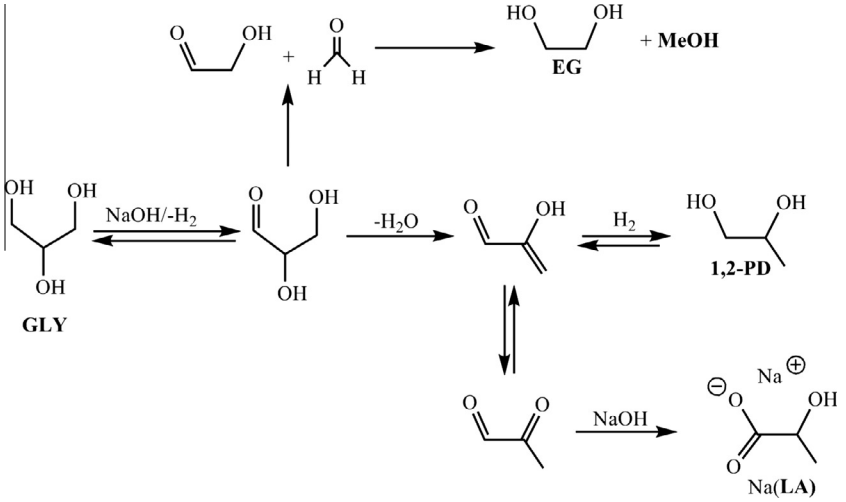

Scheme 2. Liquid GLY hydrogenolysis products.

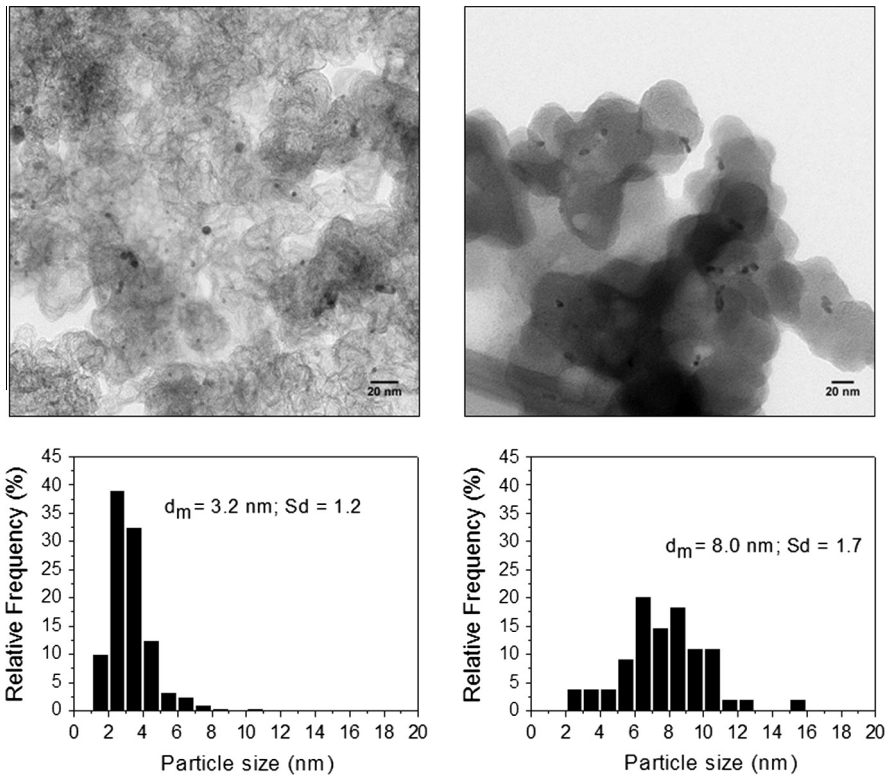

Fig. 4. HRTEM-micrographs and histograms of recovered $Pt_a@C^K$ (left) and $Pt_a@C^V$ (right) after catalysis conducted at 453 K for 4 h.

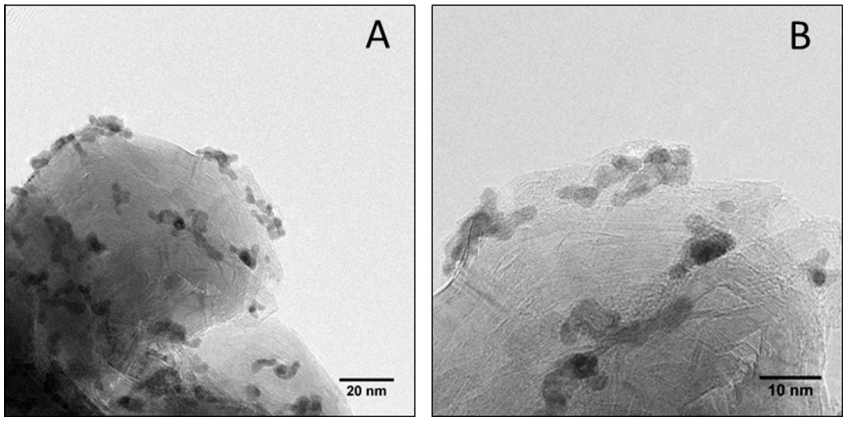

Fig. 5. HRTEM-micrographs of recovered $Pt_a@C^G$ with different magnification (A and B) after catalysis conducted at 453 K for 4 h.

The isolated supported catalysts have been characterized by HRTEM, PXRD, N_2-physisorption, and H_2-chemisorption. As a result, HRTEM analysis showed for $Pt_a@C^{K/V/G}$ Pt-NPs of <1.3 nm in size (Fig. 1) regardless of the support, while $Pt_b@C^{K/V}$ revealed a mean Pt-NP size of 2.4 ± 0.7 and 2.6 ± 0.6 nm for C^K and C^V, respectively (Fig. 2). In all the examined samples, high-angle annular dark-field scanning transmission electron microscopy (HAADF-STEM) analysis revealed homogeneous dispersions of the Pt-NPs onto the different supports (Figs. S1–S5). Accordingly, PXRD diffractograms acquired for the as-synthesized $Pt_b@C^{K/V}$ catalysts (Fig. 3) showed a small hump for the Pt(1 1 1) Bragg reflex of *fcc* Pt centered at 40.0° (2Θ) [27], while for $Pt_a@C^{K/V/G}$ catalysts, the line broadening was too large to observe the Pt(1 1 1) Bragg reflex.

The metal dispersion calculated from average particle size obtained from HRTEM observations following the equation $d_{rel(VS)} = 3.32/FE^{1.23}$ (where FE is the fraction exposed, $d_{rel(VS)} = d_{VS}/d_{at}$, ($d_{VS}$) is the volume-surface mean diameter of an assembly of particles of different sizes, and d_{at} is the atomic diameter of platinum (2.7 Å)) [28] were in accordance with the results obtained from H_2 chemisorption experiments carried out on $Pt_a@C^K$ and $Pt_b@C^K$: 91% (HRTEM)/87% (chemisorption), 58% (HRTEM)/53% (chemisorption), respectively. Analogous results were obtained with $Pt_a@C^V$ and $Pt_b@C^V$: 90% (HRTEM)/85% (chemisorption), 53% (HRTEM)/50% (chemisorption), respectively. The N_2-physisorption carried out on $Pt_{a,b}@C^K$ and $Pt_{a,b}@C^V$ showed a significant reduction of the carbon surface area of C^K and C^V, due to the reduction of the pore volume, upon supporting Pt-NPs (Table 1). When mesitylene (a-type catalysts) was used as solvent for the MVS technique, the surface area reduction was much higher compared to *n*-pentane, regardless of the carbon support used (*i.e.*, C^K (surface area reduction): 44% (mesitylene) *vs* 29% (pentane); C^V

Table 3
Average Pt-NPs' size of supported catalysts before and after GLY hydrogenolysis at 453 and 433 K.

Catalyst	Pt-NP diameter in nm				
	As-synthesized	After catalysis at 453 K		After catalysis at 433 K	
		4 h	8 h	4 h	8 h
$Pt_a@C^K$	1.3[a]	3.2[a]		5.4[b]	7.4[b]
$Pt_a@C^V$	1.3[a]	8.0[a]		6.7[b]	9.0[b]
$Pt_b@C^K$	2.4[a]		6.5[b]		
$Pt_b@C^V$	2.6[a]		10.2[b]		

[a] From HRTEM measurements.
[b] From PXRD measurements.

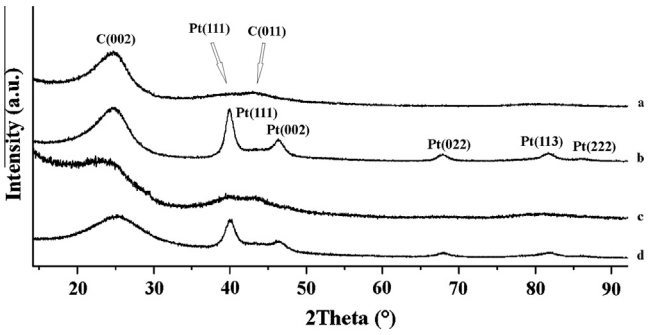

Fig. 6. PXRD diffractograms of as-synthesized $Pt_b@C^V$ (a), recovered $Pt_b@C^V$ (b), as-synthesized $Pt_b@C^K$ (c), and recovered $Pt_b@C^K$ (d).

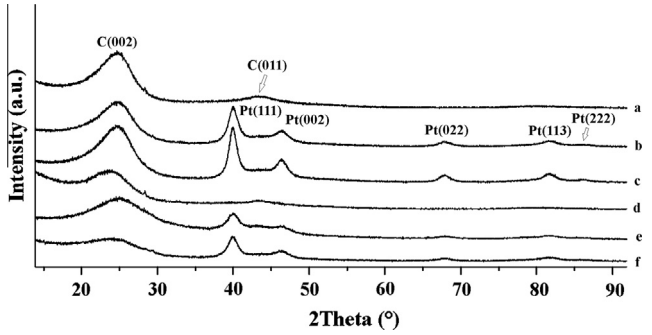

Fig. 7. PXRD diffractograms of as-synthesized $Pt_a@C^V$ (a), recovered $Pt_a@C^V$ (4 h) (b), recovered $Pt_a@C^V$ (8 h) (c), as-synthesized $Pt_a@C^K$ (d), recovered $Pt_a@C^K$ (4 h) (e), and recovered $Pt_a@C^K$ (8 h) (f).

(surface area reduction): 40% (mesitylene) *vs* 25% (pentane). A controlled heating of $Pt_a@C^K$ (2.0 °C/min) combined with an online mass spectroscopic analysis (*i.e.,* $[mesitylene\text{-}CH_3]^+$ (m/z = 105)) of the mesitylene released from the carbon support showed that at 57 °C outer pore, mesitylene is released from C^K, while mesitylene localized inside the pores is released in an extremely broad temperature range (*i.e.*, from 170 to 300 °C (Fig. S6). The average pore width distribution (*i.e.,* bimodal pore width distribution) of $C^{K/V}$ did not change upon supporting Pt.

$Pt_{a,b}@C^K$, $Pt_{a,b}@C^V$, and $Pt_a@C^G$ were used to catalyze the aqueous-phase hydrogenolysis reaction of GLY (2.4 vol%) in the presence of NaOH (0.8 M), H_2 pressure (600 psi at 303 K), and a GLY to $Pt_{(surface)}$ ratio of 1274 [29]. The catalytic reactions were performed at 453 K and 433 K in order the estimate the effect of the reaction temperature on the overall catalytic activity and chemoselectivity toward 1,2-PD which is the target organic compound.

The liquid- and gas-phase products formed in the course of the GLY hydrogenolysis reactions were analyzed by HPLC and mass spectrometry, respectively. Importantly, the carbon mass balance was in all cases >99%. The results of the catalytic screening are compiled in Table 2.

All catalytic hydrogenolysis reactions were carried out in the presence of base, since in its absence, only a very low GLY conversion was obtained (Table 1, entry 4) [6]. Regardless of the reaction temperature, the obtained liquid-phase reaction products were 1,2-PD, ethylene glycol (EG), and MeOH (not reported in Table 2) which were formed in a 1:1 molar ratio, due to a retro-aldol reaction [30] and the sodium salt of lactic acid (Na(LA)) [31,32] (Scheme 2). The gas-phase products consisted of CO, CO_2, and traces of CH_4.

Catalytic GLY hydrogenolysis reactions conducted at 453 K clearly showed for the a-type Pt catalysts, a much higher activity compared to the b-type analogs along with a lower chemoselectivity for 1,2-PD (Table 2, entries 1/7 *vs* 2/8). This lower 1,2-PD chemoselectivity found for the former catalysts is mainly due to their high aqueous-phase reforming activity (APR) (Table 2), which is expected to be higher for smaller Pt-NPs due to the higher number of edge and corner atoms [11–16]. Also, the EG formation is lower in b-type compared to a-type catalysts, while the yield of Na(LA) seems to mainly depend on the surface area of the applied support. As a result, the carbon support with the smallest surface area gave the highest amount of LA (*i.e.*, 12%). More importantly, LA is not only produced from GLY [31,32] but it is also accessible by dehydrogenation of 1,2-PD and successive reaction with base (Scheme 2). Accordingly, an independent experiment using 1, 2-PD as substrate (Table 2, entry 6) gave 23% of LA, even in the presence of H_2.

The water–gas shift (WGS) reaction [33–36] seemed slightly more favoured by $Pt@C^K$ compared to $Pt@C^V$, regardless of the initial size of the Pt-NPs, while on C^G, WGS is almost not occurring.

Analogous catalytic GLY hydrogenolysis reactions carried out at 433 K (Table 2, entries 11–20) exhibited for $Pt_a@C^K$ the highest GLY conversion (TOF = 181 h^{-1}) along with the highest chemoselectivity for 1,2-PD (73%) (Table 2, entry 11). This latter chemoselectivity dropped to 70% for a catalytic reaction lasting 8 h (entry 14). Conversely, $Pt_b@C^K$ showed under identical catalytic conditions a much lower catalytic activity (TOF = 48 h^{-1}) and chemoselectivity for 1,2-PD (60%) (entry 15). Even $Pt_a@C^V$ (entry 16) gave scarves results in terms of 1,2-PD chemoselectivity (53%). LA was formed at 433 K only by $Pt@C^V$. We recycled twice $Pt_a@C^K$ and $Pt_a@C^V$at 433 K and observed for the former catalyst a slight decrease of the catalytic activity as well as chemoselectivity (*i.e.*, 68% after the 2nd recycling experiment, entry 13), while the latter one reached a chemoselectivity of only 40% after the 2nd recycling experiment (entry 18).

In order to study the aggregation of the Pt-NP on $C^{K/V/G}$ under catalytic hydrogenolysis reaction conditions, we separated the solid catalysts from the solution after catalysis by a simple filtration at room temperature and washed the black solids with water and acetone, followed by air-drying. HRTEM-analyses of $Pt_a@C^{K/V/G}$, recovered after the catalytic reactions performed at 453 K for 4 h, were carried out and representative micrographs are shown in Figs. 4 and 5.

In Table 3 are compared the Pd-NPs' size of the different catalysts before and after GLY hydrogenolysis reaction carried out at 453 and 433 K.

The HRTEM-micrographs evidenced a significant increase of the Pt-NPs size on C^V and C^G in the course of the catalytic hydrogenolysis reactions. Most importantly under the applied reaction conditions, Pt-NPs on C^G gave a predominant amount of particles which form larger aggregates, precluding hence a reliable particle size histogram (Fig. 5). In contrast, $Pt_a@C^K$ showed after catalysis at 453 K, 4 h relatively small Pt-NPs of 3.2 ± 1.2 nm. The same trend in the Pt-NPs size was observed with b-type catalysts after

catalytic reactions conducted at the same temperature but lasting 8 h (Table 3). The Pt-NP size was determined in this latter case from the corresponding PXRD spectra (Fig. 6b and d) by the means of the Debye–Scherrer method [37] based on the Pt(111) Bragg reflex centered at 40.0° (2Θ).

An analysis of the PXRD diffractograms of recovered $Pt_a@C^{K/V}$ after hydrogenolysis reactions at 433 K lasting 4 and 8 h (Fig. 7) (Table 3) confirmed the slower sintering of Pt-NPs on C^K compared to C^V.

N_2-physisorption analysis carried out on recovered $Pt_a@C^K$ (433 K, 4 h) showed almost the same support surface area for C^K as the as-synthesized catalyst (Table 1) (*i.e.*, 743 m^2/g *vs* 775 m^2/g (as-synthesized), proving the stability of the C^K support in the course of the catalytic GLY hydrogenolysis reactions.

The stability of $Pt_a@C^{K/V}$ against Pt leaching into aqueous solution during GLY hydrogenolysis was proved by hot filtration (353 K) of the supported catalyst from solution, which was subjected to ICP-OES analysis. As a result, very low amounts of Pt in solution were detected (*i.e.*, <2 ppb for $Pt_a@C^K$ and 0.064 ppm for $Pt_a@C^V$), thus indicating the efficient anchoring of Pt-NPs on the graphite structure of $C^{K/V}$.

4. Conclusions

Well-defined Pt-NPs of controlled size (<1.3 nm and 2.4 nm), prepared by means of MVS technique, were deposited on carbonaceous supports such as Ketjen Black EC-600JD (C^K), Vulcan XC-72 (C^V), and fewer layer graphene (C^G) and applied for basic glycerol hydrogenolysis reactions carried out at 453 and 433 K. HRTEM and PXRD measurements carried out on recovered catalysts confirmed that the Pt-NP sintering is retarded on a high surface carbon support such as C^K, regardless of the initial Pt-NP size, while on C^G (lowest surface area), the strongest Pt-NP aggregation occurred, fostering the formation of lactate. The stronger control of C^K over the Pt-NP sintering compared to C^V and C^G led to: (*i*) a high chemoselectivity for 1,2-PD (73%) at 433 K (*i.e.,* at 453 K, the aqueous-phase reforming of glycerol notably decreased the 1,2-PD chemoselectivity) with a TOF of 181 h^{-1}; (*ii*) a recyclable catalysts which showed a drop of 1,2-PD chemoselectivity to 68% after the third catalytic cycle.

Acknowledgment

C.E. and R.P.J. thank MIUR-Italy (FIRB 2010; contract RBFR10BF5V) for financial support.

Appendix A. Supplementary material

Supplementary data associated with this article can be found, in the online version, at http://dx.doi.org/10.1016/j.jcat.2015.03.003.

References

[1] E. D'Hondt, S. Van de Vyver, B.F. Sels, P.A. Jacobs, Chem. Commun. (2008) 6011.
[2] M.A. Dasari, P.-P. Kiatsimkul, W.R. Sutterlin, G.J. Suppes, Appl. Catal. A: Gen. 281 (2005) 225.
[3] D. Roy, B. Subramaniam, R.V. Chaudhari, Catal. Today 156 (2010) 31.
[4] T. Miyazawa, S. Koso, K. Kunimori, K. Tomishige, Appl. Catal. A: Gen. 318 (2007) 244.
[5] A. Torres, D. Roy, B. Subramaniam, R.V. Chaudhari, Ind. Eng. Chem. Res. 49 (2010) 10826.
[6] E.P. Maris, R.J. Davis, J. Catal. 249 (2007) 328.
[7] E.P. Maris, W.C. Ketchie, M. Murayama, R.J. Davis, J. Catal. 251 (2007) 281.
[8] J. Chaminand, L. Djakovitch, P. Gallezot, P. Marion, C. Pinel, C. Rosier, Green Chem. 6 (2004) 359.
[9] T. Kurosaka, H. Maruyama, I. Naribayashi, Y. Sasaki, Catal. Commun. 9 (2008) 1360.
[10] M. Pagliaro, R. Ciriminna, H. Kimura, M. Rossi, C. Della Pina, Angew. Chem., Int. Ed. 46 (2007) 4434.
[11] J.N. Chheda, G.W. Huber, J.A. Dumesic, Angew. Chem., Int. Ed. 46 (2007) 7164.
[12] A. Wawrzetz, B. Peng, A. Hrabar, A. Jentys, A.A. Lemonidou, J.A. Lercher, J. Catal. 269 (2010) 411.
[13] R.R. Davda, J.W. Shabaker, G.W. Huber, R.D. Cortright, J.A. Dumesic, Appl. Catal. B: Environ. 56 (2005) 171.
[14] R.R. Soares, D.A. Simonetti, J.A. Dumesic, Angew. Chem., Int. Ed. 45 (2006) 3982.
[15] K. Lehnert, P. Claus, Catal. Commun. 9 (2008) 2543.
[16] H.J. Park, H.-D. Kim, T.-W. Kim, K.-E. Jeong, H.-J. Chae, S.-Y. Jeong, Y.-M. Chung, Y.-K. Park, C.-U. Kim, ChemSusChem 5 (2012) 629.
[17] C.N.R. Rao, G.U. Kulkarni, P.J. Thomas, P.P. Edwards, Chem. Eur. J. 8 (2002) 29.
[18] D.G. Lahr, B.H. Shanks, J. Catal. 232 (2005) 386.
[19] M. Bevilacqua, C. Bianchini, A. Marchionni, J. Filippi, A. Lavacchi, H. Miller, W. Oberhauser, F. Vizza, G. Granozzi, L. Artiglia, S.P. Annen, F. Krumeich, H. Grützmacher, Energy Environ. Sci. 5 (2012) 8608.
[20] B.R.S. Lemos, I.F. Teixeira, B.F. Machado, M.R.A. Alves, J.P. de Mesquita, R.R. Ribeiro, R.R. Bacsa, P. Serp, R.M. Lago, J. Mater. Chem. A 1 (2013) 9491.
[21] G. Vitulli, C. Evangelisti, A.M. Caporusso, P. Pertici, N. Panziera, S. Bertozzi, P. Salvadori, in: B. Corain, G. Schmid, N. Toshima (Eds.), Metal Nanoclusters in Catalysis and Material Science. The Issue of Size-Control, Elsevier, Amsterdam, 2008 (Chapter 32).
[22] C. Evangelisti, L.A. Aronica, M. Botavina, G. Martra, C. Battocchio, G. Polzonetti, J. Mol. Catal. A: Chem. 366 (2013) 288.
[23] C.N.R. Rao, G.U. Kulkarni, P.J. Thomas, P.P. Edwards, Chem. Soc. Rev. 29 (2000) 27.
[24] P. Paalanen, B.M. Weckhuysen, M. Sankar, Catal. Sci. Technol. 3 (2013) 2869.
[25] J.M. Campelo, D. Luna, R. Luque, J.M. Marinas, A.A. Romero, ChemSusChem 2 (2009) 18.
[26] G. Ucello-Barretta, C. Evangelisti, P. Raffa, F. Balzano, S. Nazzi, G. Marta, G. Vitulli, P. Salvadori, J. Organomet. Chem. 694 (2009) 1813.
[27] PXRD Data were Extracted from PDF-2 Containing ICDD (International Centre for Diffraction Data) Experimental Powder Data Collection. <http://www.icdd.com>.
[28] A. Borodzinski, M. Bonarowska, Langmuir 13 (1997) 5613.
[29] W. Oberhauser, C. Evangelisti, R. Psaro, F. Vizza, M. Bevilacqua, J. Filippi, A. Lavacchi, A. Marchionni, H.A. Miller, B.F. Machado, P. Serp, in: Technical Proceedings of the 2014 NSTI Nanotechnology Conference and Expo, NSTI-Nanotech 2014, Washington DC, 15–18 June 2014, vol. 3, 2014, p. 273.
[30] D.K. Sohounloue, C. Montassier, J. Barbier, React. Kinet. Catal. Lett. 22 (1983) 391.
[31] Y. Shen, S. Zhang, H. Li, Y. Ren, H. Liu, Chem. Eur. J. 16 (2010) 7368.
[32] D. Roy, B. Subramaniam, R.V. Chaudhari, ACS Catal. 1 (2011) 548.
[33] T. Bunluesin, R.J. Gorte, G.W. Graham, Appl. Catal. B: Environ. 15 (1998) 107.
[34] K.G. Azzam, I.V. Babich, K. Seshan, L. Lefferts, J. Catal. 251 (2007) 163.
[35] W. Ruettinger, X. Liu, X. Xu, R.J. Farrauto, Top. Catal. 51 (2008) 60.
[36] K.G. Azzam, I.V. Babich, K. Seshan, L. Lefferts, Appl. Catal. B: Environ. 80 (2008) 129.
[37] J.I. Langford, A.J. Wilson, J. Appl. Cryst. 11 (1978) 102.